

Fermi National Accelerator Laboratory

Studies for the ILC-IR Nb₃Sn quadrupoles

Mauricio Lopes

07/27/2007

1 Introduction

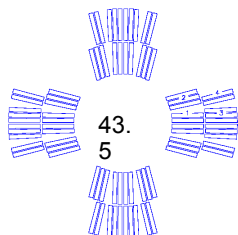
This document summarizes the results of simulations for Nb₃Sn quadrupole magnets. Different apertures and coil widths were simulated using Roxie [1]. The coils were optimized to minimize the B₆ and B₁₀ field harmonics to less than one unit (10⁻⁴) from the main field component at the reference radius. Studies related to the critical current density (J_c) were also done.

2 Simulated geometries catalog

In the following pictures it is presented the geometries that were used in the simulations followed by a short coil and cable description.

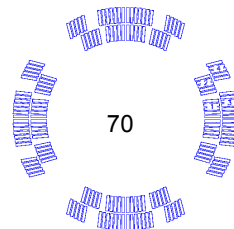
HFQA – 43.5 mm aperture:

- V1 : 14.2 mm cable, 1.0 mm strand, 2 layers: 2/2 ⁽¹⁾
- V1.1 : 14.2 mm cable, 1.0 mm strand, 2 layers: 2/1
- V2 : 14.2 mm cable, 0.7 mm strand, 2 layers: 2/2
- V2.1 : 14.2 mm cable, 1.0 mm strand, 2 layers: 2/1



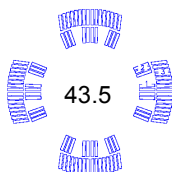
HFQC – 70.0 mm aperture:

- V1 : 7.0 mm cable, 0.7 mm strand, 2 layers: 2/1
- V2 : 7.0 mm cable, 0.7 mm strand, 2 layers: 2/2



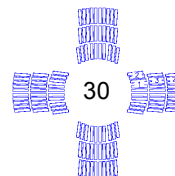
HFQB – 43.5 mm aperture:

- 7.0 mm cable, 0.7 mm strand, 2 layers: 2/1



HFQD – 30.0 mm aperture:

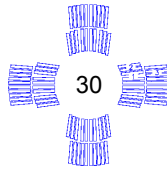
- 7.0 mm cable, 0.7 mm strand, 3 layers: 2/1/1



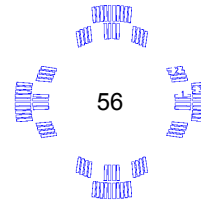
¹ Notation: NB1/NB2/NB3

NB1: number of blocks in the first layer
 NB2: number of blocks in the second layer
 NB3: number of blocks in the third layer
 (when applicable)

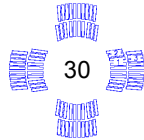
HFQE – 30.0 mm aperture:
9.8 mm cable, 0.7 mm strand, 2 layers: 2/1



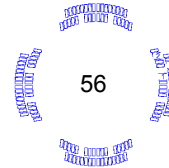
HFQK – 56.0 mm aperture:
7.0 mm cable, 0.7 mm strand, 2 layers: 2/1



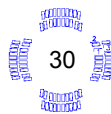
HFQF – 30.0 mm aperture:
7.0 mm cable, 0.7 mm strand, 2 layers: 2/1



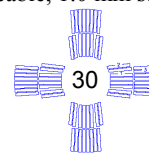
HFQL – 56.0 mm aperture:
V1 : 3.5 mm cable, 0.7 mm strand, 2 layers: 2/1
V2 : 3.5 mm cable, 0.5 mm strand, 2 layers: 2/1



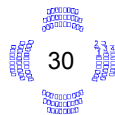
HFQG – 30.0 mm aperture:
V1 : 3.5 mm cable, 0.7 mm strand, 2 layers: 2/1
V2 : 3.5 mm cable, 0.5 mm strand, 2 layers: 2/1



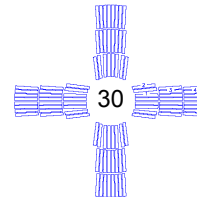
HFQM – 30.0 mm aperture:
14.2 mm cable, 1.0 mm strand, 2 layers: 2/1



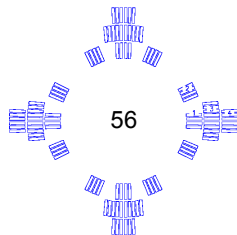
V3 : 2.1 mm cable, 0.7 mm strand, 3 layers: 2/1/1
V4 : 2.5 mm cable, 0.5 mm strand, 3 layers: 2/1/1



HFQN – 30.0 mm aperture:
14.2 mm cable, 1.0 mm strand, 3 layers: 2/1/1



HFQH – 56.0 mm aperture:
7.0 mm cable, 0.7 mm strand, 3 layers: 2/1/1



3 Cable data

As seen in the last section, different cable widths and strands diameters were used in the simulations. Eight cables, have their cross section data calculated using the standard Rutherford cable [2] formulas and parameters. Table 1 summarizes these data.

Name	Cable width [mm]	Inner height [mm]	Outer height [mm]	horizontal insulation [mm]	vertical insulation [mm]	Number of strands	Strand diameter [mm]	Cu/Sc ratio	Cabling angle [°]	Operational Temperature [K]	BcRef [T]	Jc @ BcRef [A/mm ²]	dJc/dB [A/(mm ² T)]
HFM1	14.232	1.687	1.913	0.254	0.254	28	1.012	0.85	14.5	4.2	12	2000	370
HFM2	14.083	1.133	1.356	0.254	0.254	40	0.700	0.85	14.5	4.2	12	2000	370
HFM3	9.845	1.167	1.323	0.254	0.254	28	0.700	0.85	14.5	4.2	12	2000	370
HFM4	7.019	1.189	1.301	0.254	0.254	20	0.700	0.85	14.5	4.2	12	2000	370
HFM5	3.478	1.217	1.273	0.254	0.254	10	0.700	0.85	14.5	4.2	12	2000	370
HFM6	3.500	0.862	0.917	0.254	0.254	14	0.500	0.85	14.5	4.2	12	2000	370
HFM7	2.074	1.229	1.261	0.254	0.254	6	0.700	0.85	14.5	4.2	12	2000	370
HFM8	2.491	0.870	0.909	0.254	0.254	10	0.500	0.85	14.5	4.2	12	2000	370

Table 1 - Cable data

In all cables were assumed a keystone angle of 1°.

4 Results considering analytical iron formulation

Roxie can perform the calculation of the influence of the external iron either by using an analytical method or by using a Finite Element Method (FEM).

In this section it is presented the results for the analytical formulation. This method is used to perform the coil blocks optimization in order to minimize the B_6 and B_{10} field harmonic components to less than 1 unit (10^{-4}) of the main field in the reference radius. The reference radius was assumed to be half of the aperture radius. The analytical iron radius was considered to be 10 mm more than the external radius of the coil.

Table 2 summarizes the results of this calculation. In order to have a better picture of the global results, considering the different geometries, one can define the adimensional quantity λ :

$$\lambda = \frac{B_{\max}}{G_{\max} \cdot R}$$

where G_{\max} and B_{\max} are , respectively, the maximum gradient and field taking into account the critical surface of the superconducting cable [2] and R is the aperture radius.

Figure 1 shows the plot of λ as function of w/r where w is the coil width and r is the aperture.

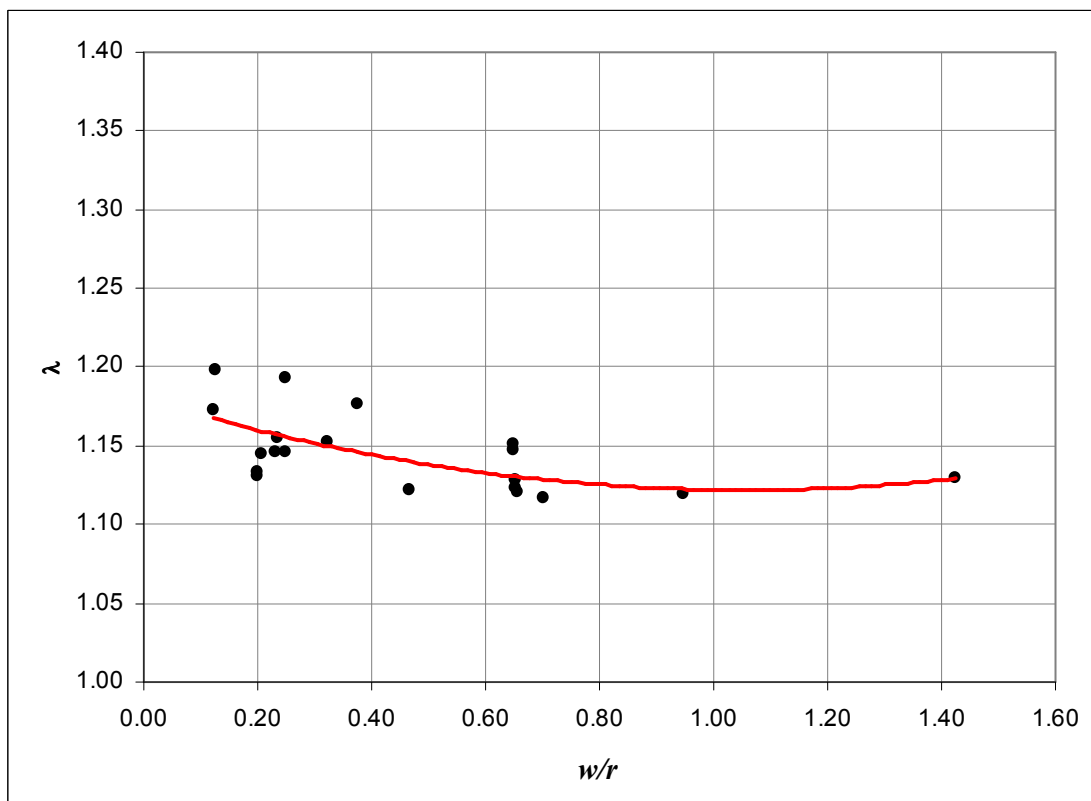


Figure 1 - λ vs. w/r . The red line represents a second order polynomial fit

Quadrupole name	Aperture [mm]	Number of layers	Aprox cable width [mm]	Strand diameter [mm]	Coil Width [mm]	I max [kA]	G_{max} [T/m]	Peak field [T]	I/Bmax	B6	B10	Layer configuration	W/R	λ
HFQ A - V1	43.5	2	14.2	1.0	28.5	31.4	426.9	10.4	3.0	0.0	-0.7	2/2	0.65	1.12
HFQ A - V1.1	43.5	2	14.2	1.0	28.5	29.0	446.3	11.0	2.6	0.0	-0.7	2/1	0.65	1.13
HFQ A - V2	43.5	2	14.1	0.7	28.2	26.0	359.2	9.0	2.9	0.0	-0.4	2/2	0.65	1.15
HFQ A - V2.1	43.5	2	14.1	0.7	28.2	22.9	399.0	10.0	2.3	0.0	-0.2	2/1	0.65	1.15
HFQ B	43.5	2	7.0	0.7	14.0	14.0	332.1	8.3	1.7	-0.1	-0.4	2/1	0.32	1.15
HFQ C - V1	70.0	2	7.0	0.7	14.0	12.2	240.5	9.5	1.3	0.0	-0.6	2/1	0.20	1.13
HFQ C - V2	70.0	2	7.0	0.7	14.0	12.1	240.8	9.5	1.3	0.0	-0.1	2/2	0.20	1.13
HFQ D	30.0	3	7.0	0.7	21.1	13.3	517.7	8.7	1.5	0.1	-0.4	2/1/1	0.70	1.12
HFQ E	30.0	2	9.8	0.7	19.7	18.7	514.2	8.6	2.2	0.1	-0.6	2/1	0.66	1.12
HFQ F	30.0	2	7.0	0.7	14.0	14.5	470.9	7.9	1.8	0.1	-0.7	2/1	0.47	1.12
HFQ G -V1	30.0	2	3.5	0.7	7.0	8.3	343.7	5.9	1.4	0.1	-0.1	2/1	0.23	1.15
HFQ G -V2	30.0	2	3.5	0.5	7.0	5.9	295.8	5.1	1.2	0.1	-0.2	2/1	0.23	1.16
HFQ G -V3	30.0	3	2.1	0.7	6.2	5.0	293.1	5.0	1.0	0.1	-0.7	2/1/1	0.21	1.14
HFQ G -V4	30.0	3	2.5	0.5	7.5	4.2	320.0	5.5	0.8	0.1	-0.7	2/1/1	0.25	1.15
HFQ H	56.0	3	7.0	0.7	21.1	14.5	241.3	7.9	1.8	0.0	0.2	2/1/1	0.38	1.18
HFQ K	56.0	2	7.0	0.7	14.0	15.1	225.7	7.5	2.0	0.0	0.1	2/1	0.25	1.19
HFQ L - V1	56.0	2	3.5	0.7	7.0	8.1	208.5	6.8	1.2	0.0	-0.9	2/1	0.12	1.17
HFQ L - V2	56.0	2	3.5	0.5	7.0	6.3	173.6	5.8	1.1	0.0	0.2	2/1	0.13	1.20
HFQ M	30.0	2	14.2	1.0	28.5	33.7	591.5	9.9	3.4	0.0	-0.2	2/1	0.95	1.12
HFQ N	30.0	3	14.2	1.0	42.7	31.2	616.3	10.4	3.0	-0.1	-0.1	2/1/1	1.42	1.13

Table 2 - Results for iron analytical formulation

As can be seen by the results shown on Table 1 and Figure 1, the maximum gradient obtained by certain geometry is limited by the relation $w/r \approx 1$ i.e., the coil width has approximately the same

size as the magnet's aperture. In these circumstances, $\lambda \approx 1.12$. This is in accordance with Todesco's estimative [3]. Figure 2 shows the reproduction of Todesco's calculation. The dependence of λ with w/r can be well fit by the expression:

$$\lambda(w, r) = a_{-1} \frac{r}{w} + 1 + a_1 \frac{w}{r}$$

with

$$a_{-1} \approx 0.04$$

and

$$a_1 \approx 0.11$$

In these circumstances the minimum of λ is 1.15.

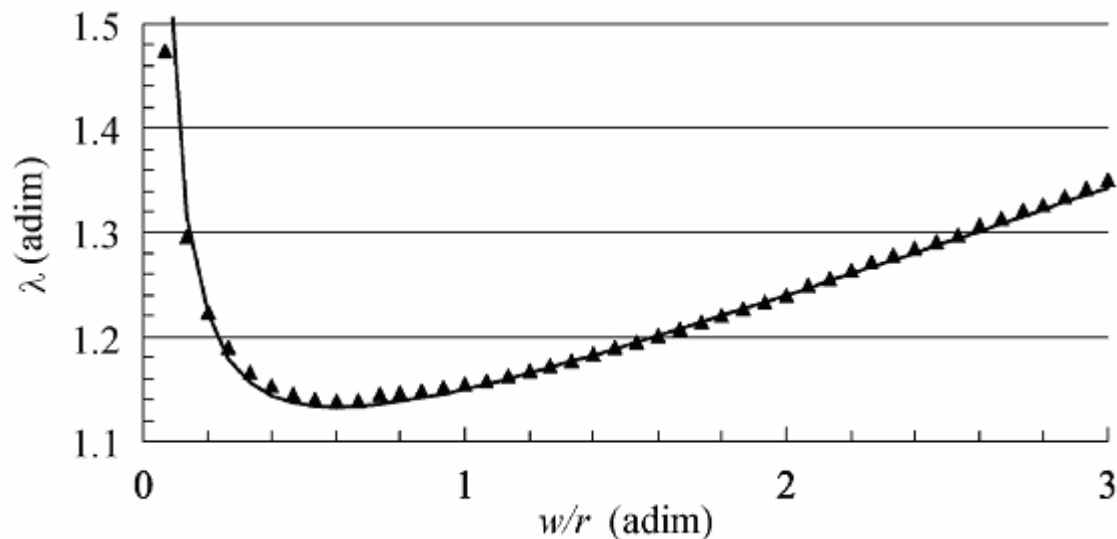


Figure 2 - Todesco's calculation for λ vs. w/r (reproduction)

However, in these calculations a constant and uniform angular current distribution was kept. In the cases presented in this note the angular current distribution had to be changed and rearranged in each case to minimize the high order harmonics, as already discussed.

5 Results considering FEM for the iron core

In this section it is presented the simulation results taking into account a FEM for the iron core. In this way, the maximum gradient value is obtained more accurately. Once again, the internal iron radius was considered as 10 mm more than coil external radius. The external iron radius was considered such as the iron width would be 300 mm. Figure 3 shows the typical magnetic field distribution in the iron core.

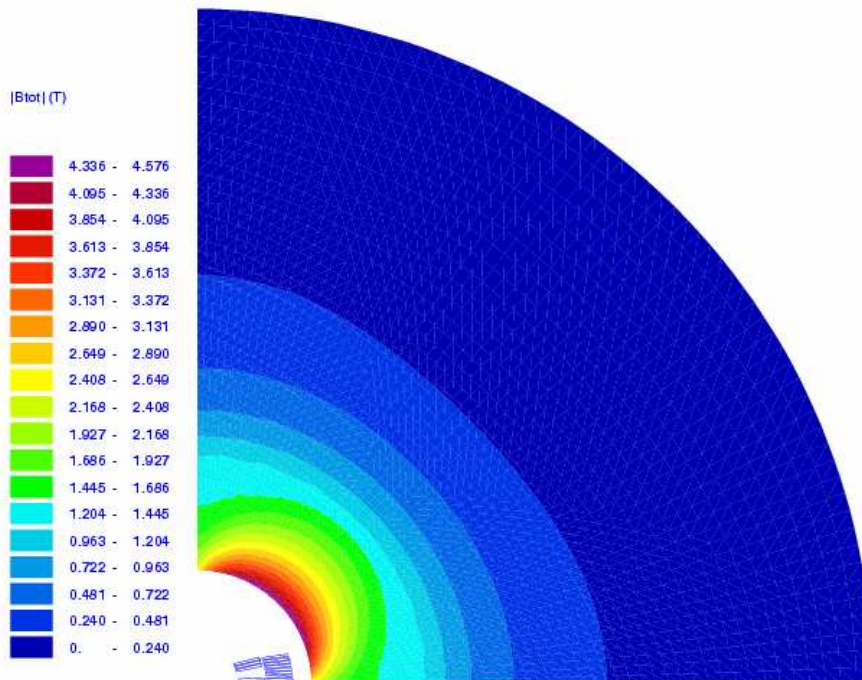


Figure 3 - Typical magnetic field distribution in the iron core.

In the same way as the previous section, one can plot λ as function of w/r (Figure 4). As can be seen, the results are essentially the same as the ones presented in Figure 1. Figure 5 shows the maximum gradient as function of w/r .

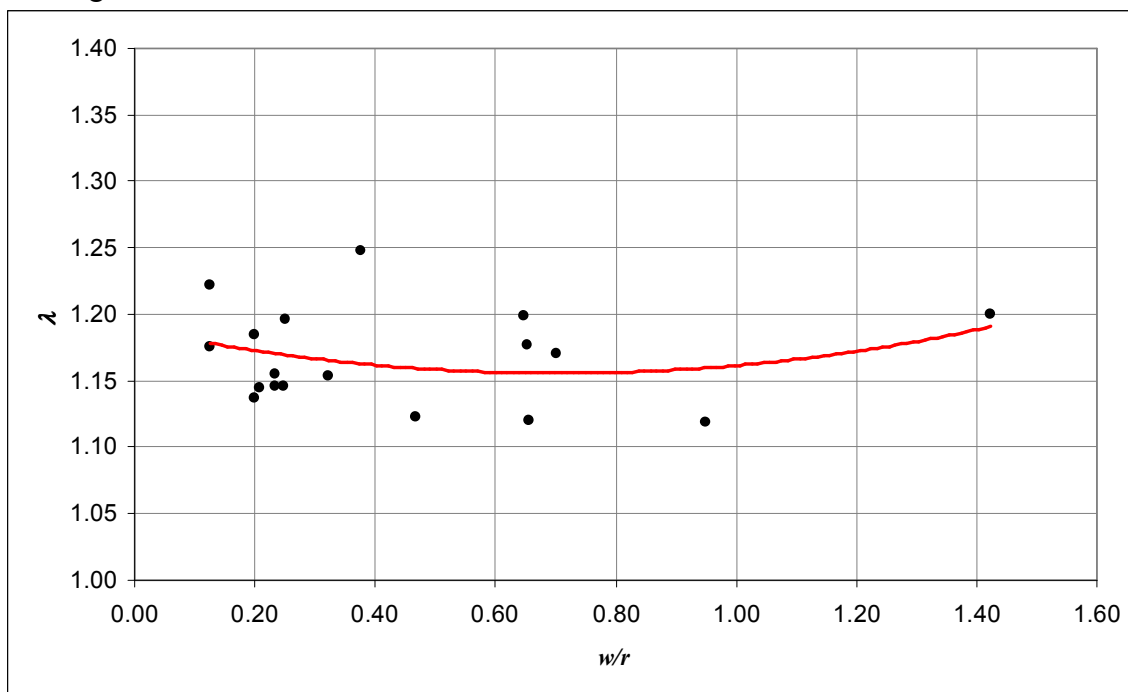


Figure 4 - λ vs. w/r using FEM for the iron core. The red line represents a second order polynomial fit

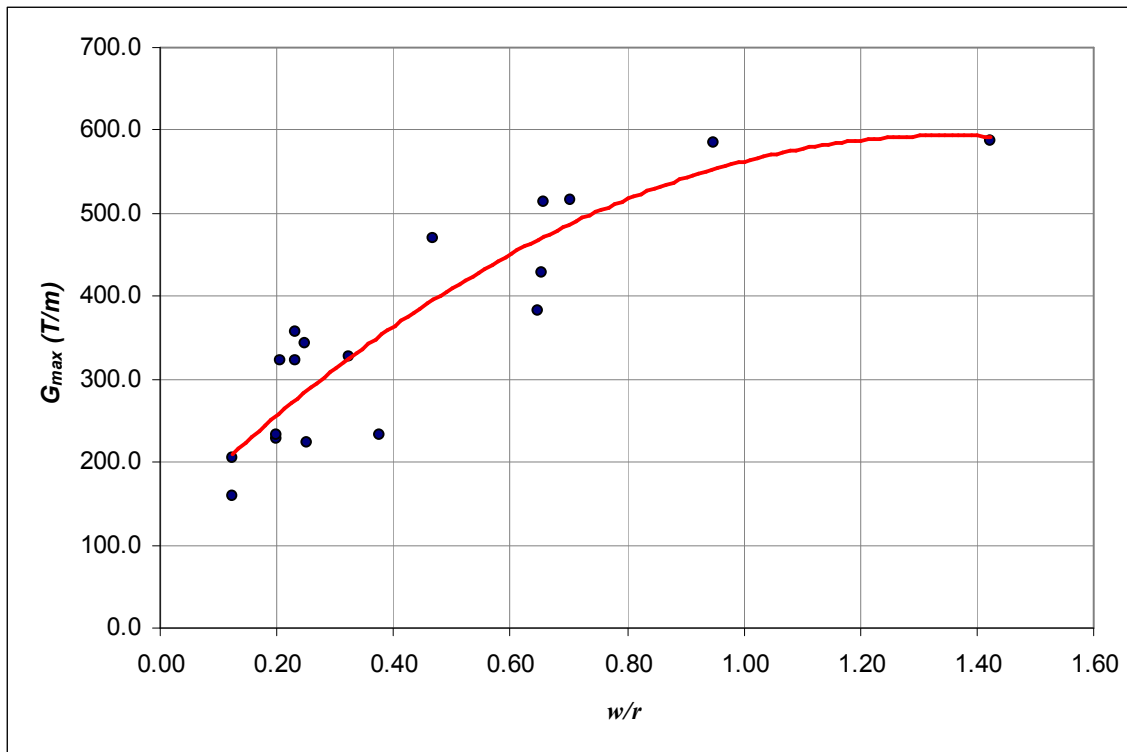


Figure 5 – Maximum gradient vs. w/r . The red line represents a second order polynomial fit

Figure 6 shows the maximum gradient as function of the coil width only for different aperture values. Figure 7 shows the same data for the 30 mm magnet aperture.

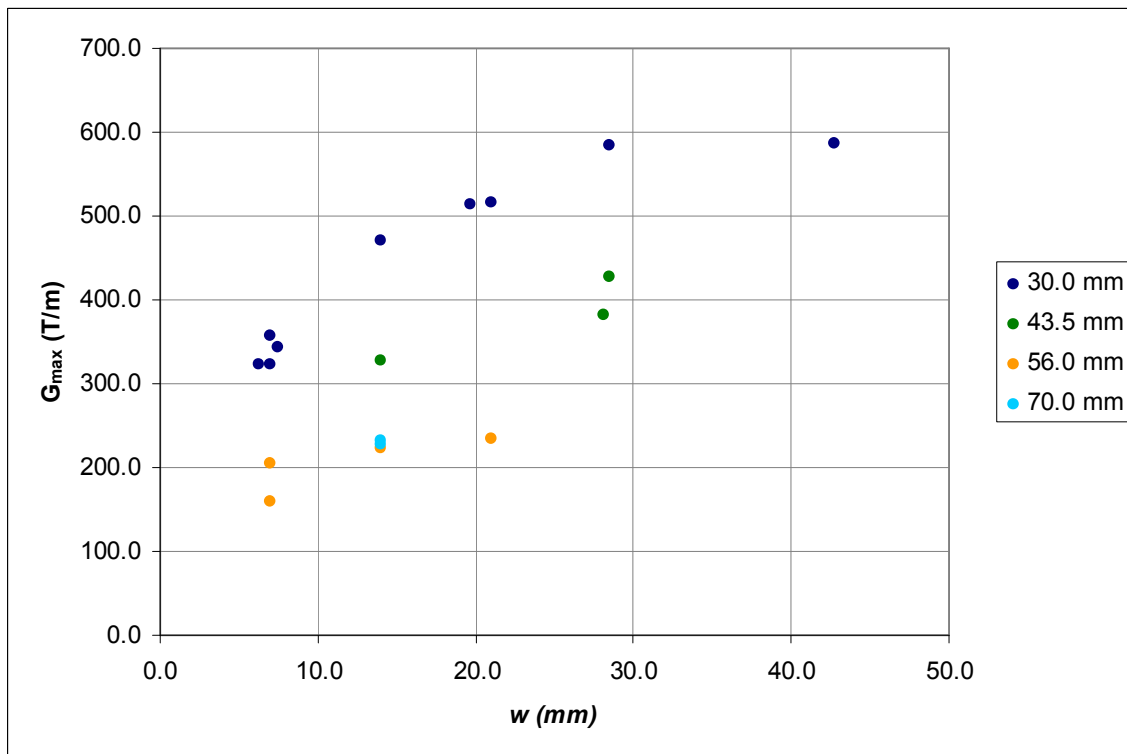


Figure 6 - Maximum gradient as function of the coil width only for different aperture values

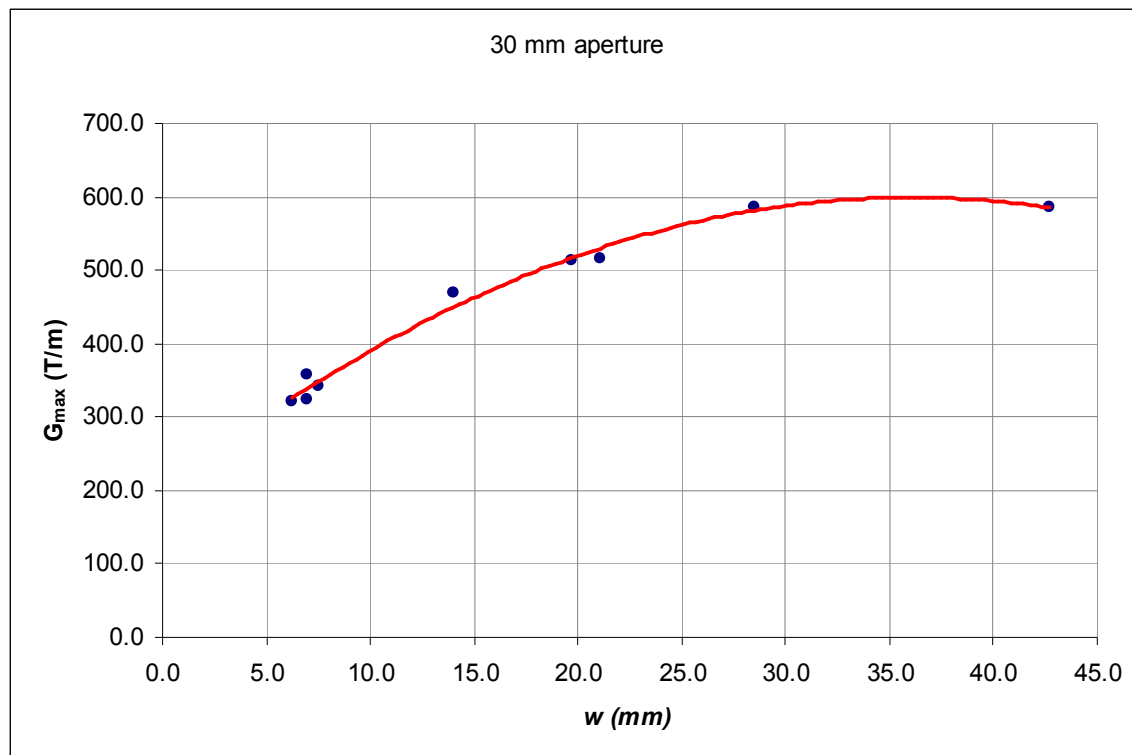


Figure 7 - Maximum gradient as function of the coil width only for 30 mm magnet aperture. The red line represents a second order polynomial fit

As can be seen, the maximum gradient for Nb_3Sn superconducting quadrupoles is around 600 T/m. For these simulations it was considered $J_c = 2000 \text{ A/mm}^2$. However Roxie, in its internal calculations, considers a first order approximation for the critical surface. It is necessary to re-run Roxie a few times and manually changing the values of the critical field (B_c), critical current density (J_c) and derivative (dJ_c/dB) in order to have a better approximation for the maximum gradient.

6 Influence of J_c in the maximum gradient

As mentioned before, Roxie performs a first order approximation for the superconductor critical surface. In order to have a better estimative of the maximum gradient due to this effect, simulations (where the J_c was varied from 1000 to 3000 A/mm^2) were done. For each new J_c , the values of B_c , local J_c and dJ_c/dB were computed (given by the transfer function of the magnet). The maximum gradient was, then, calculated. The results are presented in Figure 8. These simulations were done using the HFQE geometry.

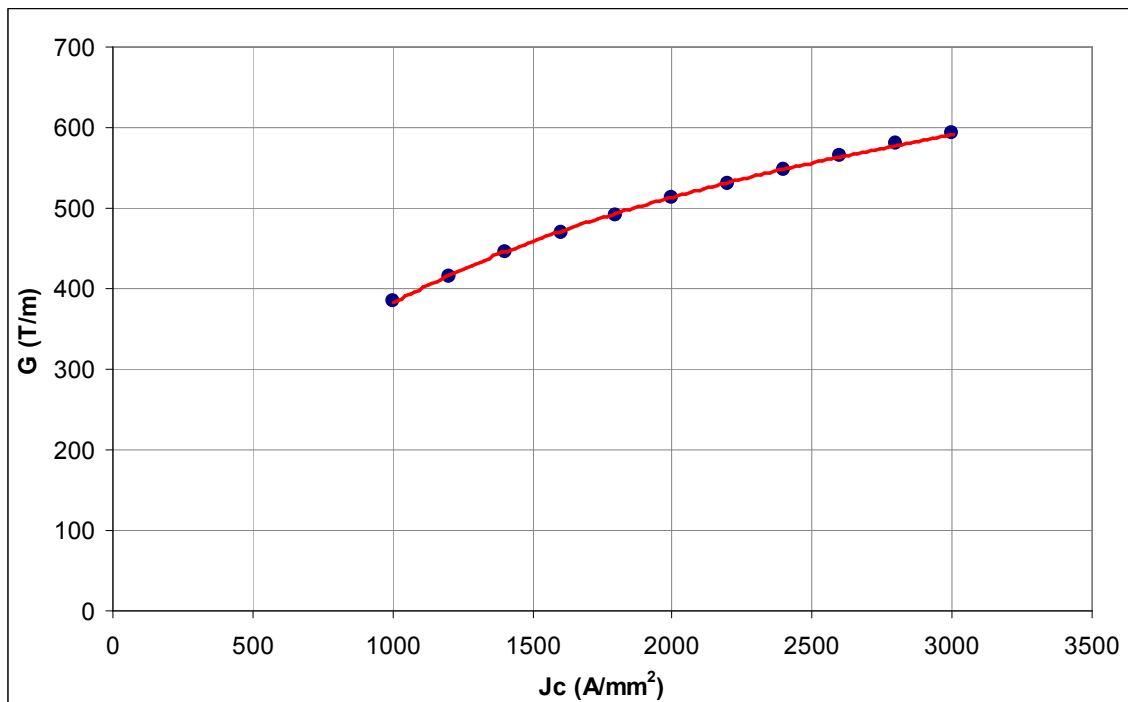


Figure 8 – maximum gradient as function of Jc. The red line represents a second order polynomial fit

7 ILC extraction quadrupole

The Interaction Region (IR) of the International Linear Collider (ILC) can be seen in Figure 9. Figure 10 shows the detailed view of the quadrupoles at IR.

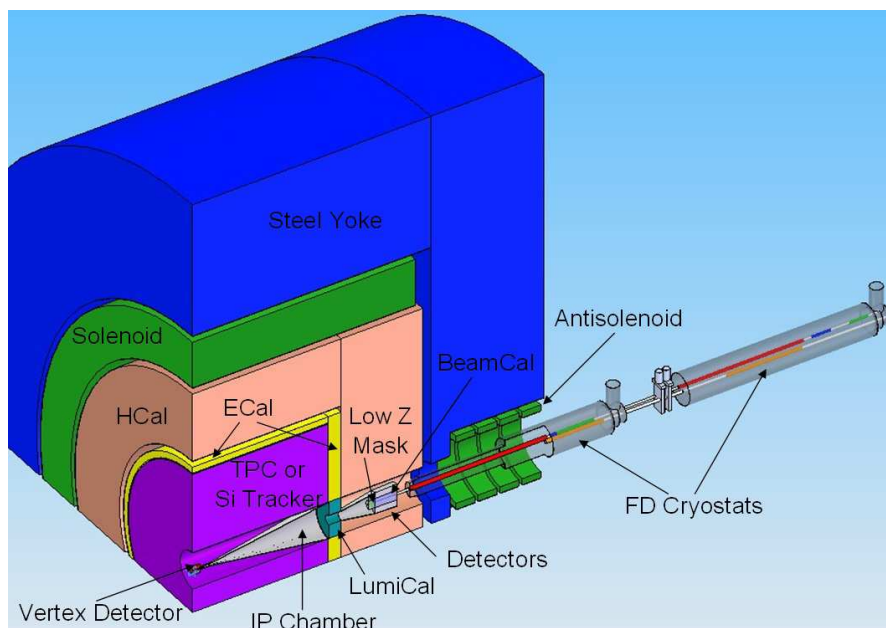


Figure 9 – IR of ILC

QD0 is the final focusing quadrupole. QDEX1 is the quadrupole for the extracted beam after the collision. More details can be found in [4].

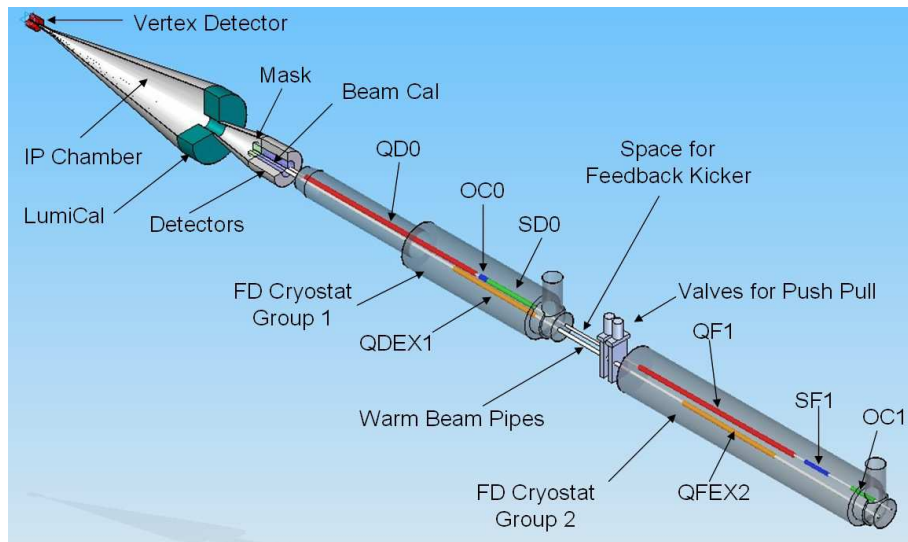


Figure 10 – Magnets details of the IR of ILC

Figure 11 shows, schematically, the distribution of the quadrupoles in the cryostats. As can be seen, QD0 and QDEX1 share the same cryostat. More over, as can be seen on Figure 9, this cryostat is inside the solenoid of the detector.

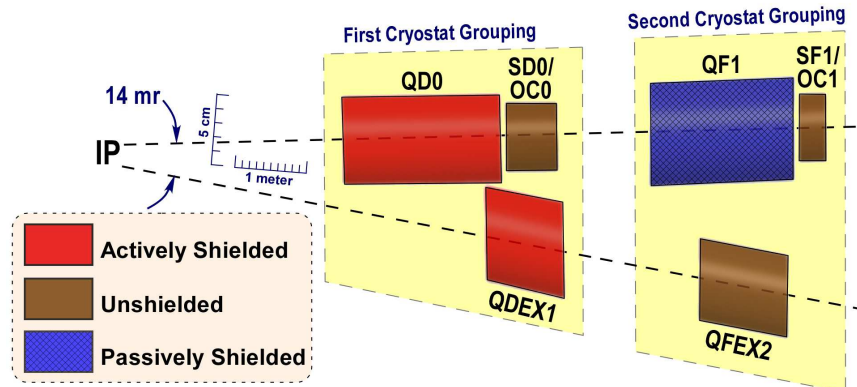


Figure 11 – Quadrupoles at IR – Cryostat view

According to [5], there were proposed 3 different apertures for QDEX1: 30, 34 and 36 mm. summarizes the specifications for these proposals. Figure 12 shows the results of simulations for these 3 apertures. In order to have a more conservative estimative, it was assumed in these simulations that $J_c = 1000 \text{ A/mm}^2$.

Aperture (mm)	Gradient (T/m)	Length (m)	L* (m) *
30	100.00	1.060	5.50
34	89.41	1.150	5.95
36	86.93	1.190	6.30

Table 3 – QDEX1 specifications

* L* = Distance between the interaction point and the quadrupole

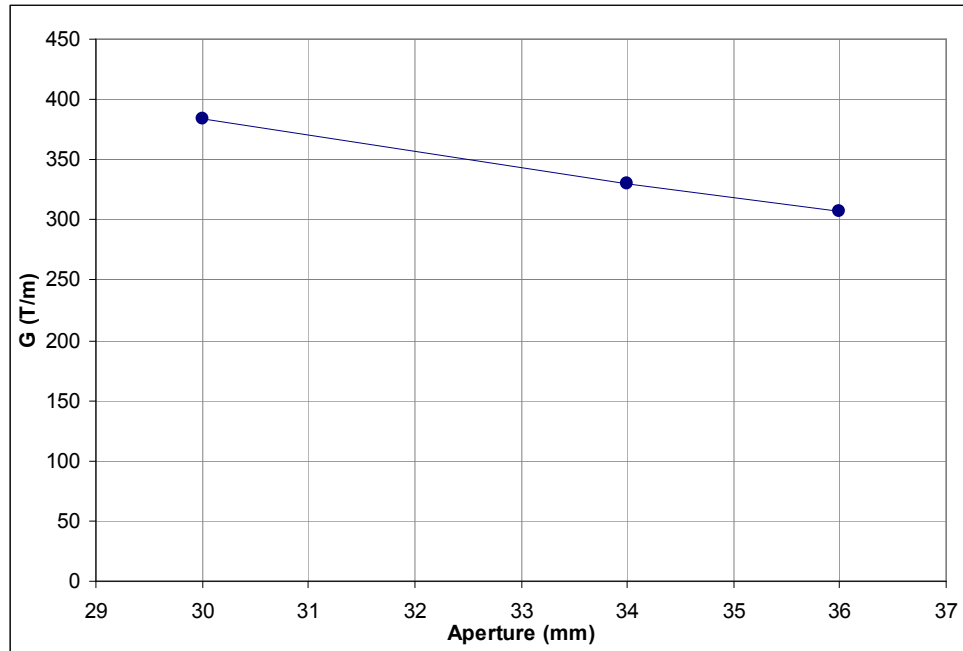


Figure 12 – maximum gradient as function of aperture for the extraction at IR of ILC. J_c was assumed to be 1000 A/mm^2

8 Conclusion

In this note the results of Nb_3Sn quadrupole simulations were presented. Different apertures and coil widths were simulated using Roxie. The coils were optimized to minimize the B_6 and B_{10} field harmonics to less than one unit from the main field component at the reference radius. The reference radius was always taken as been half of the aperture radius in each case.

Even though the ILC-IR quadrupoles do not include iron yoke, calculations with iron yoke were done in order to have a more conservative evaluation of the maximum gradient.

The influence of the critical current density (J_c) in the cable description for the maximum gradient was also calculated.

The results for the first ILC-IR quadrupole suggest that the coil width could be reduced. The next steps would be the optimization of these coils to meet the space constrains.

References

-
- [1] S. Russenschuck, “Roxie - The Routine for the Optimization of magnet X-sections, Inverse field computation and coil End design”, <http://at-mel-em.web.cern.ch/at-mel-em/> , 2007
- [2] K.-H. Mess, P. Schmüser, S. Wolf, “Superconducting accelerator magnets”, World Scientific, 1996
- [3] E. Todesco, L. Rossi, “An estimate of the maximum gradient in superconducting quadupoles”, IEEE Transactions on applied superconductivity, Vol. 17, N^o. 2, June 2007
- [4] ILC Reference Design Report, [http:// media.linearcollider.org/rdr_draft_v1.pdf](http://media.linearcollider.org/rdr_draft_v1.pdf) , 2007
- [5] Y. Nosochkov, “Preliminary extraction optics for proposed options of L*”, 2007